

Cite this: *Mater. Adv.*, 2020,  
1, 3333

## Synthesis and characterization of $\text{Cu}_3\text{SbS}_4$ thin films grown by co-sputtering metal precursors and subsequent sulfurization†

A Azizur Rahman,<sup>a</sup> Emroj Hossian,<sup>b</sup> Hetal Vaishnav,<sup>b</sup>  
Jayesh B. Parmar,<sup>b</sup> Arnab Bhattacharya<sup>b</sup> and Arun Sarma<sup>ac</sup>

$\text{Cu}_3\text{SbS}_4$  (famatinite) thin films were synthesized using a two-step process: Cu and Sb metals were first deposited by RF magnetron sputtering, followed by subsequent sulfurization. The influence of metal precursor ratio, sulfurization temperature and time on surface morphology, composition, and structural and optical properties was systematically investigated. X-ray diffraction and Raman analysis revealed the formation of  $\text{Cu}_3\text{SbS}_4$  phase thin films, where the crystallinity and phase purity improve with sulfurization temperature. Synthesis at a process temperature of 425 °C gave phase-pure  $\text{Cu}_3\text{SbS}_4$  thin film with uniform surface morphology, whereas secondary phases were formed at reaction temperatures lower than 400 °C. A temperature higher than 425 °C led to films with voids between the crystallites. The bandgap of the optimized films was measured to be 0.89 eV and 0.83 eV using UV-VIS-NIR spectroscopy and spectroscopic ellipsometry measurements, respectively. This suggests the potential use of  $\text{Cu}_3\text{SbS}_4$  as an absorber layer for thin film solar cells.

Received 6th August 2020,  
Accepted 27th October 2020

DOI: 10.1039/d0ma00574f

rsc.li/materials-advances

## Introduction

Copper antimony sulfide compounds commonly known as CAS materials are emerging semiconductors having potential applications in the field of photovoltaics,<sup>1–5</sup> thermoelectricity,<sup>6,7</sup> photo-electrochemical cells,<sup>8,9</sup> supercapacitors<sup>10,11</sup> and also as topological insulators.<sup>12</sup> This material system is composed of the elements Cu, Sb and S which are relatively earth-abundant, low cost and of low toxicity. In addition to being earth-abundant, CAS thin films with good crystalline quality can be grown at much lower temperatures of ~400 °C in contrast to well-established Cu–In–Ga–Se (CIGS) and Cu–Zn–Sn–S (CZTS) thin films.<sup>13</sup> Hence, the CAS material system has recently attracted much attention, owing to its suitable optical and electrical properties for PV applications.<sup>13,14</sup> CAS exist in four major crystal phases:  $\text{CuSbS}_2$  (chalcostibite),  $\text{Cu}_3\text{SbS}_3$  (skinnerite),  $\text{Cu}_3\text{SbS}_4$  (famatinite) and  $\text{Cu}_{12}\text{Sb}_4\text{S}_{13}$  (tetrahedrite). These semiconductor materials have bandgaps ranging from 0.5 to 2 eV, high

absorption coefficient ( $\alpha > 10^5 \text{ cm}^{-1}$ ) and show p-type electrical conductivity<sup>15</sup> which makes them ideal for photovoltaic applications. Among the four stable phases,  $\text{CuSbS}_2$  and  $\text{Cu}_3\text{SbS}_4$  have been identified as potential candidates for solar cells. Among these two compounds  $\text{CuSbS}_2$  has been widely explored for PV applications.<sup>1–3,8</sup> However, a recent theoretical investigation on the electronic structure of  $\text{CuMCh}_2$  ( $\text{M} = \text{Sb, Bi; Ch} = \text{S, Se}$ ) predicts that  $\text{CuSbS}_2$  is unlikely to display the desired transport properties for use in solar cells as it has an indirect bandgap with low hole mobility.<sup>16</sup> The same authors have preferred the use of the related materials like  $\text{Cu}_3\text{SbS}_3$  and  $\text{Cu}_3\text{SbS}_4$  provided they exhibit the requisite optical and transport properties. Similarly, Yu *et al.*,<sup>17</sup> have done a computational study for identifying materials with a suitable solar absorption profile and identified  $\text{CuSbS}_2$  and  $\text{Cu}_3\text{SbS}_4$  as worthy for investigation as solar cell materials.<sup>17</sup> Additionally, they showed that  $\text{Cu}_3\text{SbS}_4$  exhibits slightly higher spectroscopic limited maximum efficiency (SLME) of 25%, than  $\text{CuSbS}_2$  (22.9%).<sup>17</sup> Thus, it is of utmost important to investigate the  $\text{Cu}_3\text{SbS}_4$  phase in order to understand its suitability for solar applications and come up with scalable deposition methods.

$\text{Cu}_3\text{SbS}_4$  phase has a reported direct optical bandgap in the range of 0.4 eV to 1 eV, high optical absorption coefficient ( $\alpha > 10^4 \text{ cm}^{-1}$ ) and p-type electrical conductivity.<sup>17–19</sup> Most of the reported work on  $\text{Cu}_3\text{SbS}_4$  is on materials only in the form of micro-structures<sup>20–22</sup> and nanostructures<sup>23–26</sup> synthesized by chemical routes. There are only few reports on the synthesis of  $\text{Cu}_3\text{SbS}_4$  in thin film form.<sup>4,27–31</sup> In spite of a variety of approaches

<sup>a</sup> School of Advanced Sciences (SAS), Vellore Institute of Technology-Chennai campus, Chennai – 600127, Tamil Nadu, India<sup>b</sup> Department of Condensed Matter Physics and Materials Science, Tata Institute of Fundamental Research, Colaba, Mumbai – 400005, India. E-mail: arnab@tifr.res.in<sup>c</sup> North East Centre for Technology Application and Reach (NECTAR), Viswakarma Bhawan, Shaheed Jeet Singh Marg, New Delhi – 110016, India

† Electronic supplementary information (ESI) available. See DOI: 10.1039/d0ma00574f



available for the synthesis of  $\text{Cu}_3\text{SbS}_4$ , the presence of secondary phases co-existing with these materials and the non-uniform surface morphology still remains a challenge limiting practical use.<sup>31</sup> Hence, studies on thin film growth of  $\text{Cu}_3\text{SbS}_4$  are necessary to understand both fundamental growth mechanisms and the influence of various deposition parameters on the properties of these films. Among the different available techniques, RF magnetron sputtering is suitable for developing high-quality thin films with an advantage of scaling to large area; however, the processing of  $\text{Cu}_3\text{SbS}_4$  through this route is still unexplored.

In this work, we report a two-stage process to develop phase-pure  $\text{Cu}_3\text{SbS}_4$  thin films. As a first step the metal precursors (Cu and Sb) were co-sputtered by RF magnetron sputtering on a sapphire substrate. Later these sputtered films were sulfurized under vacuum at different temperatures. The synthesized materials were characterized by different experimental techniques, like GIXRD, Raman spectroscopy, SEM, TEM, UV-VIS-NIR spectroscopy and spectroscopic ellipsometry measurements. The influence of metal precursor ratio, sulfurization temperature and time on the structural, morphological, compositional, and optical properties are discussed, and the optimum conditions for the formation of phase-pure  $\text{Cu}_3\text{SbS}_4$  thin films identified.

## Method

The growth of  $\text{Cu}_3\text{SbS}_4$  involves a two-step process. In the first step, metal precursors were co-sputtered onto the sapphire substrate, and then the samples were sulfurized in a vacuum-sealed quartz ampoule. RF magnetron sputtering was used to co-sputter copper and antimony metal precursors on the substrate. A schematic representation of the two-stage growth process is shown in ESI† (Fig. S1). The Cu and Sb targets (Testbourne Ltd, purity ~99.99%) were fixed at a tilt angle of 45° and located at a mean distance of 7 cm from the substrate. The substrate was kept at a temperature of 200 °C for better film adhesivity and the substrate holder was rotated to ensure uniform deposition. A plasma of high purity (99.998%) Ar with a background pressure of  $\sim 10^{-2}$  mbar and at a flow of 30 sccm was used during the co-sputtering process. Cu–Sb films of 250 nm thickness with different [Cu]/[Sb] ratios were sputtered on to the substrate and the elemental composition of the grown films was analyzed by EDX (energy dispersive X-ray spectroscopy) in a scanning electron microscope. A table showing the influence on RF power on the [Cu]/[Sb] ratio is shown in the ESI† (Table S1). The sputtered Cu–Sb thin films were then sealed in a quartz ampoule with excess sulfur (0.1 g). Prior to the sulfurization process, the quartz ampoule of 15 mm diameter and 30 cm length was cleaned with HF solution, thoroughly rinsed in deionized water and purged with high purity Ar gas to remove any traces of oxygen and other contaminants. The sputtered films along with sulfur were evacuated to a pressure of  $\sim 6 \times 10^{-5}$  mbar using a diffusion pump backed by rotary pump and sealed in the quartz ampoule. The vacuum-sealed precursors in quartz ampoule were heated in a single zone wire-wound tubular furnace at different temperatures ranging from 200 °C

to 450 °C to complete the sulfurization process. The temperature of the furnace was ramped at a rate of 10 °C min<sup>-1</sup>, and then the samples were allowed to cool down to the ambient through natural heat-loss processes.

The structural properties of the films were determined using a Rigaku Smartlab 9 kW rotating anode X-ray diffractometer at 1° incidence in a grazing incidence XRD (GIXRD) mode. Raman spectroscopy measurements were performed on the samples using a WITec Alpha 300R confocal Raman microscope. Detailed studies on microstructure and composition of the films were performed using a field emission scanning electron microscope (FESEM) operated at a voltage ranging from 5–20 kV (Zeiss Ultra FESEM). Optical transmission and reflection spectra were measured at normal incidence using a Cary 5000 spectrophotometer. Variable angle spectroscopic ellipsometry (VASE) were performed using an alpha-SE ellipsometer (J.A. Woollam Co.). High-resolution transmission electron microscopy (HRTEM) images and selected area electron diffraction (SAED) patterns were recorded using a 200 kV FEI Tecnai-20 system.

## Result and discussion

### X-ray diffraction

The Cu:Sb ratio and sulfurization time were optimized previously in separate experiments (see ESI† for details). The conditions of these parameters—Cu:Sb metal ratio of 1:1 and dwell time of sulfurization process of 60 minutes—were kept constant for all temperature studies. Fig. 1 shows GIXRD patterns of CAS thin films sulfurized at temperatures varying from 200 °C to 450 °C. The GIXRD data demonstrate that the diffusion of sulfur vapor and formation of phases strongly depend on temperature. Sputtered Cu–Sb films sulfurized at higher temperatures like 450 °C and 425 °C exhibit prominent diffraction peaks at  $2\theta = 28.7^\circ, 29.9^\circ, 33.3^\circ, 47.8^\circ, 56.6^\circ$  which can be attributed to (112), (103), (200), (204), (312) planes of  $\text{Cu}_3\text{SbS}_4$  (famatinite) phase (JCPDS No. 00-035-0581). Peaks of

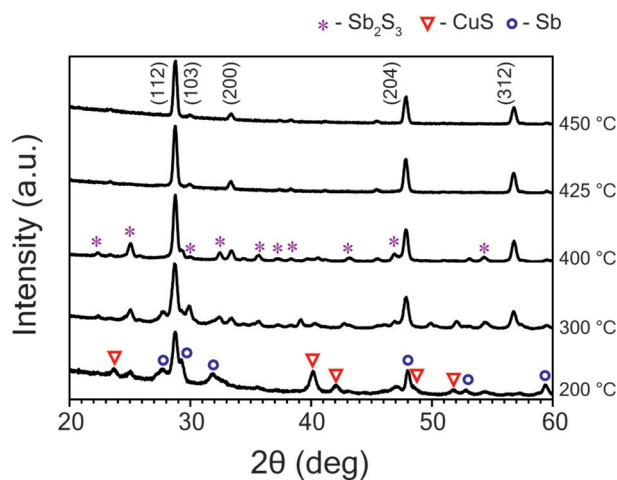


Fig. 1 GIXRD patterns of samples sulfurized at temperatures of 200 °C to 450 °C; numbers indicate (*hkl*) indices of  $\text{Cu}_3\text{SbS}_4$ , secondary phases of metallic Sb,  $\text{Sb}_2\text{S}_3$  and CuS are marked with different symbols.



other binary and ternary phases of these material system were not observed in this temperature range. Similarly, the GIXRD profile of films sulfurized at lower temperature range like 400 °C and 300 °C show diffraction peaks of binary  $\text{Sb}_2\text{S}_3$  (stibnite) and  $\text{CuS}$  (covellite) phases in addition to the dominant  $\text{Cu}_3\text{SbS}_4$  phase. The  $\text{Sb}_2\text{S}_3$  and  $\text{CuS}$  peaks are denoted by '\*' and '▼' symbols, respectively, in Fig. 1. For the films sulfurized at a much lower temperature of 200 °C, apart from the  $\text{CuS}$ ,  $\text{Sb}_2\text{S}_3$  phases, unreacted  $\text{Sb}$  metal (marked with a '◊' symbol) was observed as well. Decrease in sulfurization temperature leads to an increase in the percentage of  $\text{CuS}$  phase, which is also evident from the GIXRD profile. The formation of  $\text{CuS}$  phase and peaks from unreacted  $\text{Sb}$  might be due to inadequate thermal energy that make metal inter-diffusion and distribution of sulfur vapor difficult. The full width at half maximum (FWHM) for (112) plane of  $\text{Cu}_3\text{SbS}_4$  decreased from 0.68° to 0.29°, indicating an improvement of crystalline quality with increase in temperature from 200 °C to 450 °C. The films were found to exhibit a tetragonal crystal structure with calculated lattice parameters  $a = 0.538$  nm and  $c = 1.075$  nm which are close to the reported lattice parameter values of the tetragonal  $\text{Cu}_3\text{SbS}_4$  phase.<sup>30</sup> The average particle size of these films, estimated from Scherrer's formula for (112) reflection, was found to increase from 12 nm to 30 nm with increasing temperature from 200 °C to 450 °C.

### Raman spectroscopy

Raman spectroscopy measurements were performed on grown thin films using 532 nm laser excitation. The incident laser power was kept low ( $\sim 1$  mW) in order to avoid structural modification or damage of the films as laser-induced surface changes have been observed in Cu based thin films at high optical flux levels.<sup>31,32</sup> Raman scattering results for samples sulfurized at different temperatures are shown in Fig. 2. The spectra obtained for samples sulfurized in the temperature regime of 450 °C to 300 °C (Fig. 2(a)–(d)) have the main Raman modes located at 244, 273, 317 and 344  $\text{cm}^{-1}$ . These peaks are in good agreement with the characteristic modes of  $\text{Cu}_3\text{SbS}_4$  phase as reported in literature and RUFF database (RRUFF ID: R11022).<sup>21,29</sup> Further lower frequency peaks positioned at 71, 90, 133, 143  $\text{cm}^{-1}$  for  $\text{Cu}_3\text{SbS}_4$  phase were observed as also recently reported.<sup>32</sup> In addition to the above peaks, one mode observed at 496  $\text{cm}^{-1}$  does not match any of the possible binary and ternary phases of the CAS system. The Raman spectra of samples sulfurized at temperatures higher than 400 °C show only the modes of dominant  $\text{Cu}_3\text{SbS}_4$  phase. However, thin films sulfurized at a lower temperature of 300 °C show a mode at 472  $\text{cm}^{-1}$  which is due to the presence of  $\text{CuS}$  phase. Raman modes of only  $\text{CuS}$  (472  $\text{cm}^{-1}$ ) and  $\text{Sb}$  (113 and 152  $\text{cm}^{-1}$ ) were observed in the sample sulfurized at 200 °C. The absence of  $\text{CuS}$  phase in Raman modes of the films sulfurized at temperatures above 400 °C is in corroboration with XRD results.

### Surface morphology

The surface morphology of these films was evaluated using FESEM imaging. Fig. 3 shows the significant effect of sulfurization temperature on the microstructure and surface morphology

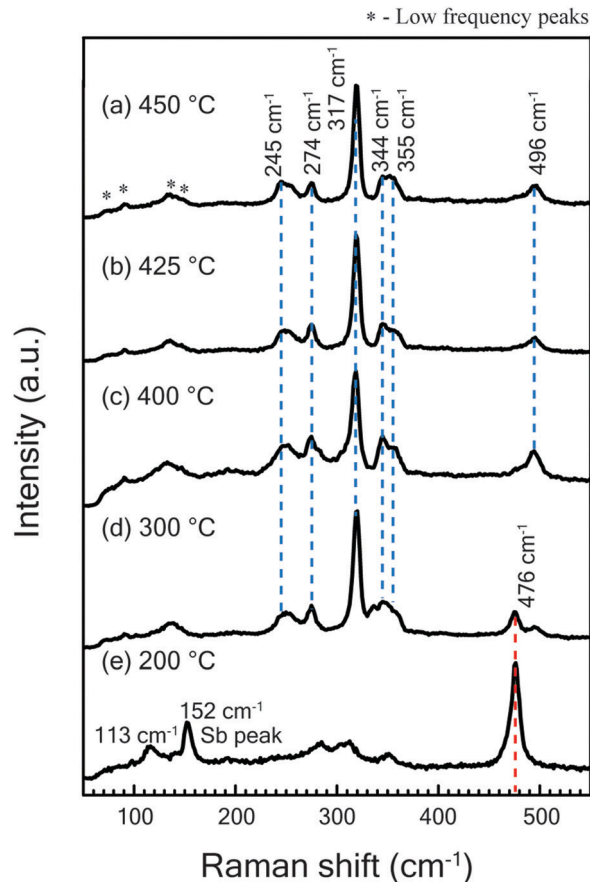


Fig. 2 (a) Raman spectra measured at room temperature at laser power  $\sim 1$  mW for thin films sulfurized at temperatures (a) 450 °C (b) 425 °C (c) 400 °C (d) 300 °C (e) 200 °C.

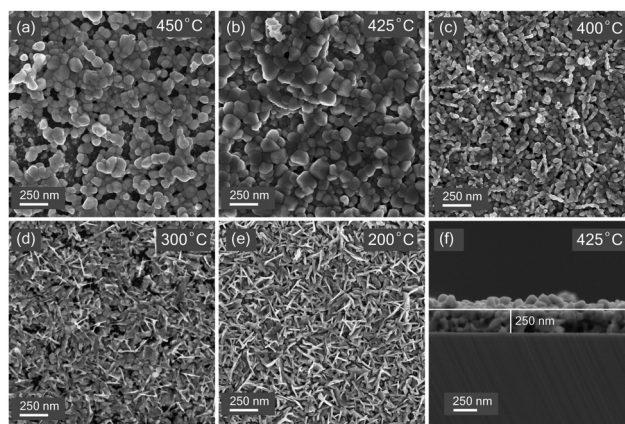


Fig. 3 Scanning electron microscope images thin films sulfurized at temperatures (a) 450 °C (b) 425 °C (c) 400 °C (d) 300 °C (e) 200 °C (f) cross-sectional SEM image of sample sulfurized at 425 °C.

of films. Films sulfurized at 450 °C (Fig. 3(a)) show a discontinuous surface with lots of voids in between the grains. Decreasing the temperature to 425 °C (Fig. 3(b)) leads to the formation of continuous uniform layers with grains of size ranging from 100–500 nm. Further decrease in temperature leads to the formation of finer



grains and promotes vertical morphological growth. Vertical flakes growth mode was observed for the samples sulfurized at 200 °C. EDX point measurements on such vertical flakes reveal the compositions of the Cu<sub>3</sub>SbS<sub>4</sub> compound. A similar morphology has been previously seen in CuS films.<sup>33,34</sup> SEM observations suggest that continuous films with uniform surface morphology can be obtained at a temperature of 425 °C. The cross-sectional FESEM image (Fig. 3(e)) of the film sulfurized at 425 °C shows a thickness of 250 nm.

### Optical properties

The optical transmittance  $T(\lambda)$  and reflectance  $R(\lambda)$  spectra of Cu<sub>3</sub>SbS<sub>4</sub> thin films sulfurized at different temperatures against wavelength are shown in Fig. 4. Transmittance and reflectance spectra show strong absorption region in the optical range of 1.3 to 1.5 μm, which can be attributed to the onset of the fundamental absorption edge of Cu<sub>3</sub>SbS<sub>4</sub> thin films as reported in the literature.<sup>28,29</sup> The weak absorption region in the range of 0.5 to 1.3 μm range arises due to the presence of the Sb<sub>2</sub>S<sub>3</sub> impurity phase. The absorption edge seen in the range of 0.5 to 1.3 μm becomes more prominent for the samples grown at lower temperatures which is in corroboration with XRD and Raman spectroscopy results. Similarly, the reflectance spectra for samples sulfurized at lower temperatures like of 300 °C and 400 °C show peaks in the range of 0.8 to 1.2 μm range because of the presence of Sb<sub>2</sub>S<sub>3</sub> phase.

Additional studies to determine the optical constants of the phase-pure Cu<sub>3</sub>SbS<sub>4</sub> thin film grown at 425 °C were conducted using variable angle spectroscopic ellipsometry (VASE). The ellipsometry study was not performed on other samples because of the presence of impurity phases. The measurements were carried out in the spectral range of 250–1500 nm. The psi ( $\Psi$ ) and delta ( $\Delta$ ) parameters were measured at 50°, 55°, 60°, 65° and 70° incidence angles (see ESI† for details). The roughness layer was modelled using a Bruggeman effective medium approximation. To obtain better fit results between the experimental and

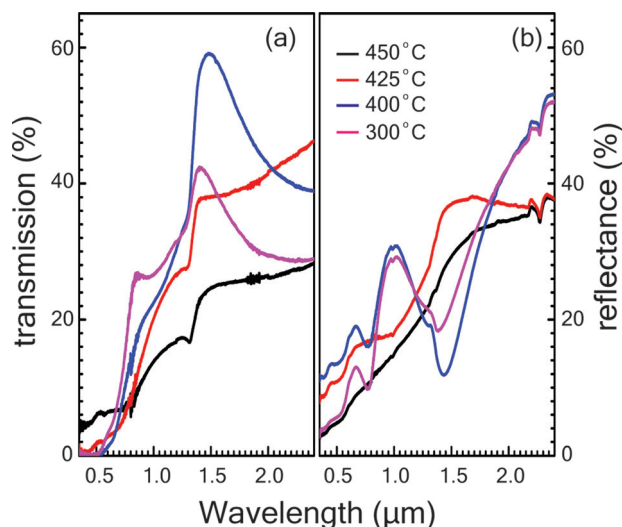


Fig. 4 Transmittance and reflectance spectra of thin films sulfurized at different temperatures.

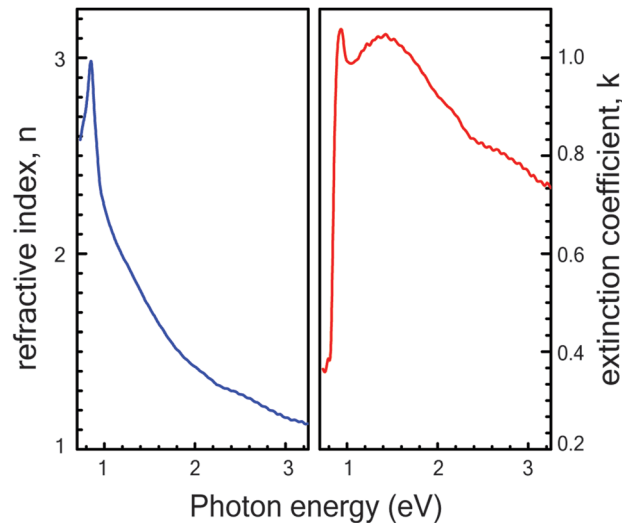


Fig. 5 Refractive index ( $n$ ) and extinction coefficient ( $k$ ) as a function of photon energy for a phase-pure Cu<sub>3</sub>SbS<sub>4</sub> thin film grown at 425 °C.

model data, mean squared error (MSE) value was kept below 10. The plots of real ( $n$ ) and imaginary ( $k$ ) part of the refractive index are shown in Fig. 5 for the film grown at 425 °C were the result of the best-fit  $\Psi$  and  $\Delta$  between the experimental data and those generated by the model. Both the refractive index ( $n$ ) and the extinction coefficient ( $k$ ) show an abrupt increase in the range of 0.7 to 0.9 eV. This can be attributed to the optical transition near the fundamental bandgap  $E_g$ , which is in agreement with the values obtained by absorption spectroscopy. The refractive index has a peak value at 0.9 eV, beyond which the  $n$  value decreases gradually to 1.1 at 3.2 eV. The extinction coefficient ( $k$ ) also shows a pronounced peak of 1.05 at 1.4 eV then the drops to 0.7 at 3.25 eV.

The optical absorption coefficient ( $\alpha_\lambda$ ) of the phase-pure Cu<sub>3</sub>SbS<sub>4</sub> thin film was evaluated by both UV-VIS-NIR spectroscopy and ellipsometry techniques. In UV-VIS-NIR spectroscopy, the absorption coefficient was calculated using the equation,  $\alpha_\lambda = \ln((1 - R_\lambda)/T_\lambda)/t$ , using the value of  $R_\lambda$  and  $T_\lambda$  extracted from the transmittance and reflectance spectra of the sample. The thickness was determined from a cross-sectional SEM image, and estimated to be 250 nm. For the spectroscopic ellipsometry case, the absorption coefficient  $\alpha_\lambda$  was obtained by applying the formula  $\alpha_\lambda = 4\pi k/\lambda$  to the SE-derived  $k$  values. The optical bandgap of the phase-pure Cu<sub>3</sub>SbS<sub>4</sub> thin film was then estimated by plotting  $(\alpha h\nu)^2$  versus  $h\nu$  (the Tauc plot) and taking the intercept. The  $(\alpha h\nu)^2$  versus  $h\nu$  plots estimated by both UV-VIS-NIR spectroscopy and ellipsometry for the optimized sample grown at 425 °C are shown in Fig. 6. (The Tauc plots of the other films sulfurized at different temperatures are shown in the ESI† as Fig. S5). The bandgap was determined to be 0.83 eV and 0.89 eV for ellipsometry and UV-VIS-NIR spectra respectively by linearly extrapolating  $(\alpha h\nu)^2$  vs.  $h\nu$  near the absorption edge of Tauc plot. These measurements show that the band edge of the film is appropriate for use as an absorber layer in thin-film solar cells.



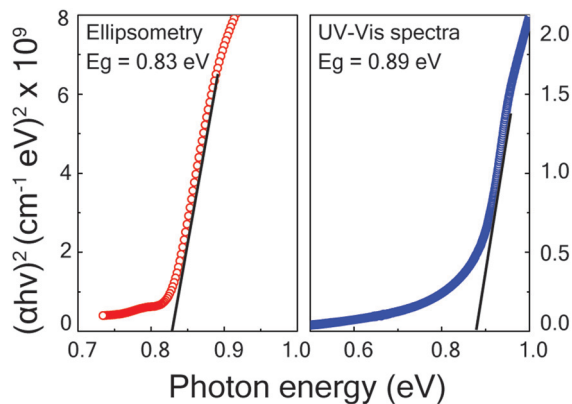


Fig. 6 Tauc plot showing linearly extrapolated band edge obtained from spectroscopic ellipsometry and UV-VIS-NIR spectroscopy for samples sulfurized at a temperature of 425 °C.

### High resolution transmission electron microscopy

The synthesized films were further characterized by high-resolution transmission electron microscopy (HR-TEM). Fig. 7(a) shows an HRTEM image of  $\text{Cu}_3\text{SbS}_4$  sample sulfurized at a temperature of 425 °C. Samples for TEM imaging were prepared by exfoliating the  $\text{Cu}_3\text{SbS}_4$  films directly on to the TEM copper grid. The exfoliated layer exhibits averaged inter-planar distances of 0.53 nm and 0.49 nm, corresponding to the (002) and (101) planes. The representative selected area diffraction (SAED) pattern in Fig. 7(c) shows sharp diffraction spots, which can be indexed to the [111] zone axis. Similarly, Fig. 7(d) shows the HRTEM image of the vertical flakes which are sulfurized at a temperature of 200 °C, and exhibit an inter-planar distance of 0.32 nm and 0.16 nm which corresponds to

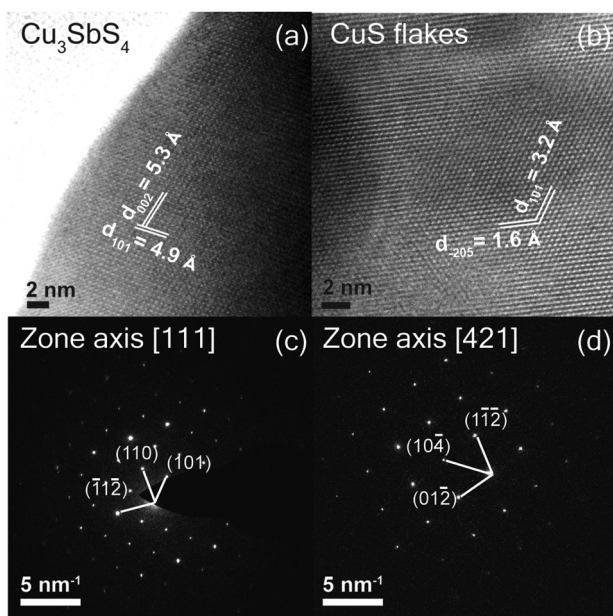


Fig. 7 High resolution TEM image of (a)  $\text{Cu}_3\text{SbS}_4$  thin films sulfurized at 425 °C (b) CuS vertical flakes, sulfurized at 200 °C, (c) SAED pattern of  $\text{Cu}_3\text{SbS}_4$  thin film (d) CuS flakes.

CuS. SAED pattern of the samples also shows sharp diffraction spots which can be indexed to the [421] zone axis of CuS.

## Conclusion

$\text{Cu}_3\text{SbS}_4$  thin films were prepared by co-sputtering of metal precursors and subsequent sulfurization at temperatures from 200–450 °C. Significant improvement in structural and optical properties was seen at higher sulfurization temperatures. Uniform, phase-pure  $\text{Cu}_3\text{SbS}_4$  films were obtained at 425 °C. These films had a tetragonal crystal structure with the lattice parameters  $a = 0.538$  nm and  $c = 1.075$  nm, and X-ray FWHM of  $0.29^\circ$  for the (112) plane. The direct optical band gap of these film was found to be in the range of 0.83–0.89 eV. The two-stage deposition process involving co-sputtering followed by sulfurization is scalable to large areas, and our results suggest that such films would be useful as an absorber layer in solar cells.

## Conflicts of interest

There are no conflicts to declare.

## Acknowledgements

We would like to acknowledge the support of Nilesh Kulkarni of TIFR, for assistance with X-ray diffraction measurements and the TIFR electron microscopy facility for TEM and SEM imaging. The work at TIFR was supported by internal grant 12P0165.

## Notes and references

- W. Septina, S. Ikeda, Y. Iga, T. Harada and M. Matsumura, *Thin Solid Films*, 2014, **550**, 700–704.
- S. Suehiro, K. Horita, M. Yuasa, T. Tanaka, K. Fujita, Y. Ishiwata, K. Shimano and T. Kida, *Inorg. Chem.*, 2015, **54**, 7840–7845.
- Y. C. Choi, E. J. Yeom, T. K. Ahn and S. I. Seok, *Angew. Chem., Int. Ed.*, 2015, **54**, 4005–4009.
- N. D. Franzer, N. R. Paudel, C. Xiao and Y. Yan, IEEE 40th Photovoltaic Specialist Conference (PVSC), 2014, pp. 2326–2328.
- G. H. Albuquerque, K. J. Kim, J. I. Lopez, A. Devaraj, S. Manandhar, Y. S. Liu, J. Guo, C. H. Chang and G. S. Herman, *J. Mater. Chem. A*, 2018, **6**(18), 8682–8692.
- V. Kumar Gudelli, V. Kanchana, G. Vaitheeswaran, A. Svane and N. E. Christensen, *J. Appl. Phys.*, 2013, **114**, 223707.
- E. J. Skoug, J. D. Cain and D. T. Morelli, *Appl. Phys. Lett.*, 2011, **98**, 261911.
- C. Yan, Z. Su, E. Gu, T. Cao, J. Yang, J. Liu, F. Liu, Y. Lai, J. Li and Y. Liu, *RSC Adv.*, 2012, **2**, 10481–10484.
- M. Han, J. Jia and W. Wang, *J. Alloys Compd.*, 2017, **705**, 356–362.
- V. K. Mariappan, K. Krishnamoorthy, P. Pazhamalai, S. Sahoo and S. J. Kim, *Electrochim. Acta*, 2018, **275**, 110–118.



- 11 K. Ramasamy, R. K. Gupta, H. Sims, S. Palchoudhury, S. Ivanov and A. Gupta, *J. Mater. Chem. A*, 2015, **3**, 13263–13274.
- 12 Y. Wang, H. Lin, T. Das, M. Hasan and A. Bansil, *New J. Phys.*, 2011, **13**, 085017.
- 13 B. Krishnan, S. Shaji and R. E. Ornelas, *J. Mater. Sci.: Mater. Electron.*, 2015, **26**, 4770–4781.
- 14 R. Ornelas-Acosta, S. Shaji, D. Avellaneda, G. Castillo, T. D. Roy and B. Krishnan, *Mater. Res. Bull.*, 2015, **61**, 215–225.
- 15 K. Ramasamy, H. Sims, W. H. Butler and A. Gupta, *Chem. Mater.*, 2014, **26**, 2891–2899.
- 16 D. J. Temple, A. B. Kehoe, J. P. Allen, G. W. Watson and D. O. Scanlon, *J. Phys. Chem. C*, 2012, **116**, 7334–7340.
- 17 L. Yu, R. S. Kokenyesi, D. A. Keszler and A. Zunger, *Adv. Energy Mater.*, 2013, **3**, 43–48.
- 18 C. T. Crespo, *J. Phys. Chem. C*, 2016, **120**, 7959–7965.
- 19 J. Van Embden, K. Latham, N. W. Duffy and Y. Tachibana, *J. Am. Chem. Soc.*, 2013, **135**, 11562–11571.
- 20 S. Blöß and M. Jansen, *Z. Naturforsch. B*, 2003, **58**, 1075–1078.
- 21 K. Aup-Ngoen, T. Thongtem and S. Thongtem, *Mater. Lett.*, 2012, **66**, 182–186.
- 22 G. Chen, W. Wang, J. Zhao, W. Yang, S. Chen, Z. Huang, R. Jian and H. Ruan, *J. Alloys Compd.*, 2016, **679**, 218–224.
- 23 J. Van Embden and Y. Tachibana, *J. Mater. Chem.*, 2012, **22**, 11466–11469.
- 24 C. An, Y. Jin, K. Tang and Y. Qian, *J. Mater. Chem.*, 2003, **13**, 301–303.
- 25 L. Shi, C. Wu, J. Li and J. Ding, *J. Alloys Compd.*, 2017, **694**, 132–135.
- 26 Q. Wang, J. Li and J. Li, *Phys. Chem. Chem. Phys.*, 2018, **20**, 1460–1475.
- 27 M. Nair, Y. Pena, J. Campos, V. Garcia and P. Nair, *J. Electrochem. Soc.*, 1998, **145**, 2113–2120.
- 28 U. Chalapathi, B. Poornaprakash, H. Cui and S.-H. Park, *Superlattices Microstruct.*, 2017, **111**, 188–193.
- 29 U. Chalapathi, B. Poornaprakash and S.-H. Park, *Ceram. Int.*, 2017, **43**, 5229–5235.
- 30 A. Pfitzner and S. Reiser, *Z. Kristallogr. - Cryst. Mater.*, 2002, **217**, 51–54.
- 31 P. Fernandes, A. Shongalova, A. da Cunha, J. Teixeira, J. Leitão, J. Cunha, S. Bose, P. Salomé and M. Correia, *J. Alloys Compd.*, 2019, **797**, 1359–1366.
- 32 A. A. Rahman, E. Hossain, H. Vaishnav, A. Bhattacharya and A. Sarma, *Semicond. Sci. Technol.*, 2019, **34**(10), 105026.
- 33 A. D. Savariraj, K. K. Viswanathan and K. Prabakar, *Electrochim. Acta*, 2014, **149**, 364–369.
- 34 Y. Chen, C. Davoisne, J. M. Tarascon and C. Guéry, *J. Mater. Chem.*, 2012, **22**(12), 5295–5299.

